

UNDERWATER STEREO USING REFRACTION-FREE IMAGE SYNTHESIZED FROM LIGHT FIELD CAMERA

Kazuto Ichimaru Hiroshi Kawasaki

Kyushu University, Japan

ABSTRACT

There is a strong demand on capturing underwater scenes without distortions caused by refraction. Since a light field camera can capture several light rays at each point of an image plane from various directions, if geometrically correct rays are chosen, it is possible to synthesize a refraction-free image. In this paper, we propose a novel technique to efficiently select such rays to synthesize a refraction-free image from an underwater image captured by a light field camera. In addition, we propose a stereo technique to reconstruct 3D shapes using a pair of our refraction-free images, which are central projection. In the experiment, we captured several underwater scenes by two light field cameras, synthesized refraction free images and applied stereo technique to reconstruct 3D shapes. The results are compared with previous techniques which are based on approximation, showing the strength of our method.

Index Terms— Stereo vision, Refraction, Light field, Underwater shape reconstruction

1. INTRODUCTION

Underwater scene acquisition is an important research topic for various areas, such as underwater construction, marine biology, swimming analysis to name a few. For those purposes, 3D shape reconstruction is most important, and thus, many techniques have been researched and developed. In terms of 3D reconstruction, passive stereo using two RGB cameras is commonly used in the air, because of its simplicity and stability. Since ordinary cameras are usually perspective, which means central projection, most stereo techniques also assume the central projection, which enables 1) efficient correspondence search using epipolar constraint, 2) linear solution on calibration, and 3) shape reconstruction by triangulation. However, underwater images are not central projection because of refraction, and thus, it is difficult to apply common stereo techniques to underwater scene.

To overcome the problem, analytical solution to estimate light path of refraction by solving high order simultaneous equations is proposed [1]. However, solving such equations requires high computational cost and it also remains ambiguities. On the other hand, approximation based technique to synthesize a refraction-free image is proposed [2]. Although the synthesized refraction-free image can be treated as central projection at predefined depth, approximation error increases when object depth becomes far from the depth.

Recently, light field imaging draw a wide attention for its potential on post-focusing, single view stereo and so on. Since a light field data is a collection of multiple light rays from various directions including non-central rays at each point on image plane, refraction-free image can be created by choosing a certain light ray from a bundle of rays at each point. In the paper, we propose a technique to find geometrically correct light rays from a light field data to synthesize a refraction-free image. Our method is implemented as a pixel warping on a captured light field image, thus, calculation time is comparable to approximation based approach. In addition, we propose a stereo technique using a pair of refraction-free images to reconstruct 3D shapes of underwater environment. In the experiment, we captured several underwater scenes by two light field cameras and conducted stereo technique to reconstruct 3D shapes. The results are compared with previous techniques, which are based on approximation model, successfully showing the strength of our method.

2. RELATED WORK

There are generally two approaches to handle refraction between the water and the air. The one is geometric approach [1, 3, 4] and the other is approximation-based approach [2, 5, 6, 7]. Geometric approach considers physical model of refraction to trace light rays, and applies forward / backward projection to render 2D images from 3D objects. In those methods, several parameters are necessary to be calibrated, such as refractive index, distance between camera and the water and normal of refractive interface. Agrawal *et al.* introduced a polynomial formulation for the model and efficient initial value computation method as well as analytical forward projection by 4-th order equation [1]. Sedlazeck and Koch proposed underwater SfM to directly recover 3D shapes without explicit calibration using efficient energy function for bundle adjustment by considering virtual camera [3]. Kawahara *et al.* proposed a pixel-wise varifocal camera model [4]. Note that most of the geometric approaches introduce special models to represent refraction effects, which is not a central projection model, and thus, general stereo method cannot be applied.

Approximation-based approach usually converts an original image to a central projection image. Ferreira *et al.* proposed an approximation-based technique to make refraction-free image by applying lens distortion model, and showed some results on stereo vision [2]. Bleier and Nüchter [5], Kawasaki *et al.* [6], and Ichimaru *et al.* [7] applied active

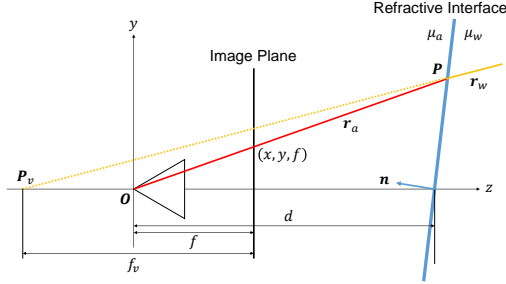


Fig. 1. Illustration of approximation-based algorithm.

method based on approximation-based approach. Since those techniques assume specific depth, severe distortion occurs if the actual depth is far from the predefined depth.

Recently, light field imaging technique draw a wide attention. In image processing task, Lu *et al.* used light field images with CNN for depth map restoration to cope with turbidity of water [8], and Li *et al.* used them for reflection removal [9]. Jeon *et al.* proposed an accurate depth map estimation method using light field camera [10]. Zhang *et al.* proposed plenoptic SfM technique [11]. Kutulakos and Steger achieved reconstruction of static transparent objects by light field imaging [12]. Wetzstein *et al.* used light field probes for normal and shape reconstruction of dynamic transparent objects [13]. Skinner and Roberson used light field camera for single-view underwater 3D reconstruction, but they ignored refraction [14]. Among wide variety of light field research, synthesis of refraction-free image has not been studied yet.

3. REFRACTION REMOVAL ALGORITHM

In this section, we first introduce conventional ways to make refraction-free image (Sec. 3.1), and then, introduce proposed method based on light field imaging (Sec. 3.2).

3.1. Virtual focus and lens distortion for approximation

Let a camera coordinate system be a pinhole model with focal length f (Fig. 1). A planar refractive surface is placed in front of the camera with depth d and normal \mathbf{n} . Both sides of the refractive surface are filled with transparent medium with different refractive indices μ_a and μ_w .

When a light ray \mathbf{r}_a is observed at (x, y, f) on the image plane, the ray is backtracked to \mathbf{P} on the refractive surface. As the ray is refracted on the refractive surface, the original direction \mathbf{r}_w of the ray can be calculated based on Snell's law. If the original ray did not refract, it intersects with optical axis at $\mathbf{P}_v = \mathbf{P} + t\mathbf{r}_w$ with appropriate coefficient t . Then we can define virtual focal length $f_v = f + |P_{vz}|$, as the system becomes central projection model.

However, since f_v depends on $\mathbf{r}_a = [x, y, f]^T$, it varies with location on the image (That is why [4] introduced pixel-wise varifocal camera model). Several approximation-based approaches apply lens distortion model to convert original image into central projection image [5, 6, 7] by using f_v and distortion coefficients, which are estimated by minimizing re-projection error. Usually, radial and tangential distortion

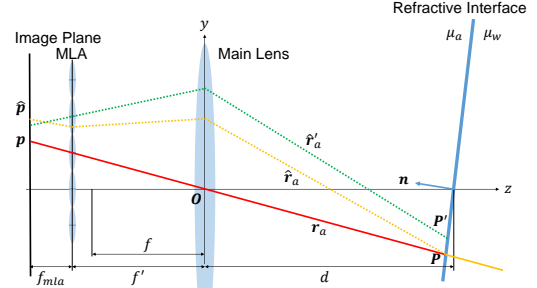


Fig. 2. Illustration of proposed algorithm. Orange line represents necessary ray, and green line represents selected ray.

model are used to represent the lens distortion, however, they can only approximate refraction at certain specific depth. Thus, approximation error increases as target depth varies from predefined depth [7], especially, when the refractive interface is slanted, approximation error is biased to specific direction, which leads to severe error.

3.2. Ray selection from light field image

To overcome the conventional distortion-free image synthesis technique based on approximation approach, we use light field image. Let a light field camera consist of a single large lens (main lens), micro lenses aligned on a plane (micro lens array; MLA) and image plane behind the MLA plane, as shown in Fig. 2. Main lens, MLA and image plane are parallel and all lenses are assumed to follow thin lens model. In the figure, f is a focal length of main lens, f_{mla} is that of MLA and f' is a distance between main lens and MLA. Note that focal length f is not equal to flange back f' unlike pinhole camera model, however, a distance between MLA and image plane is equal to f_{mla} . The system represents physical light field camera model, instead of two-plane model.

When a light ray \mathbf{r}_a is observed at \mathbf{p} on the image plane, the ray is backtracked to \mathbf{P} on the refractive surface. If there were no refraction, the ray comes along straight line, however, it is refracted and reaches to another location $\hat{\mathbf{p}}$. Therefore, by moving a color of $\hat{\mathbf{p}}$ onto location \mathbf{p} , we can make refraction-free image.

In terms of calculation of $\hat{\mathbf{p}}$, we use ray tracing technique with thin lens model. We can analytically compute which micro lens and which pixel the ray reaches. However information of the ray is often lost because not all ray passes center of the micro lens. Thus, instead of using the computed $\hat{\mathbf{p}}$, we select the closest ray from neighbor rays which passes through the center of the micro lens. A distance between necessary ray and selected ray is defined as below:

$$D = |\mathbf{P}' - \mathbf{P}| + \lambda \cos^{-1}(\hat{\mathbf{r}}'_a \cdot \hat{\mathbf{r}}_a), \quad (1)$$

where $\hat{\mathbf{r}}'_a$ is direction of selected ray, $\hat{\mathbf{r}}_a$ is direction of necessary ray, \mathbf{P}' is intersection between $\hat{\mathbf{r}}'_a$ and the refractive surface and λ is a weight. Once a ray which minimizes D is found, \mathbf{p} is assigned a color of a pixel the ray reached.

In practice, since it is almost impossible to calibrate f , it is assumed to be equal to f' . The second term of D always

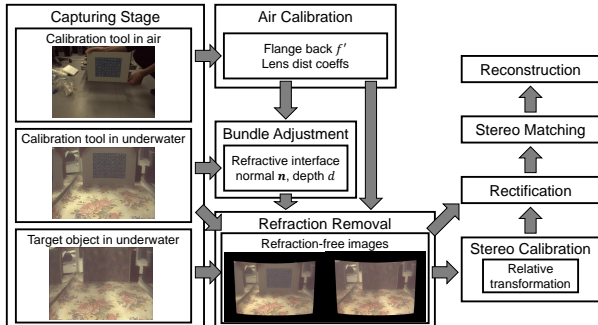


Fig. 3. Schematic of refraction-free stereo.

becomes zero based on simple calculation, thus, only the distance from the intersections is minimized.

4. IMPLEMENTATION

4.1. Refraction-free image synthesis

To achieve efficient computation, we divided the synthesis process into two parts, such as light path computation and pixel warping part, because light path computation is just once required through the entire process. In light path computation part, we analytically compute light path for each micro lens to find pixel-to-pixel correspondences, unless necessary light path goes to the outside the aperture. We get locations of all micro lenses manually. Once pixel-to-pixel correspondences are obtained, we apply weighted average and super-sampling for better image quality. For weighted average calculation, we extract several rays in ascending order of D and average their color intensities according to reciprocal number of each D . For super-sampling, we increase the number of pixel-to-pixel correspondences by computing subpixel rays. The number of rays for average and the super-sampling ratio are changed in our implementation. We finally obtain a pixel warping map based on weight for average and super-sampling for each pixel.

In pixel warping part, we simply use the pre-computed pixel warping map to light field image and final image with specified resolution is obtained by bilinear interpolation.

4.2. Underwater stereo using refraction-free image

Two light field cameras are used to conduct underwater stereo. Overview of the process is shown in Fig. 3. First, calibration tools (e.g., chess patterned board) are captured both in the air and the liquid and 2D locations of feature points are obtained. Second, real flange back f' and lens distortion coefficients of the cameras are calibrated with images captured in the air. Cameras' real lens distortion effect is removed from all images at this stage. Calibration of relative transformation of the cameras is not necessary here, thus air images can be captured separately. Third, d and n of the refractive interface are calibrated by bundle adjustment using the method of [1]. Then, refraction-free images are synthesized using proposed algorithm with obtained parameters f' , d , and n . Using the image set, relative position and orientation between camera pair are

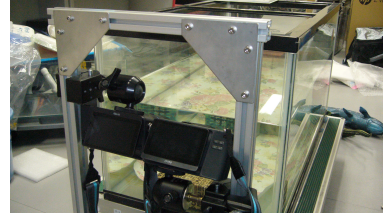


Fig. 4. Appearance of the experimental setup.



Fig. 5. Examples of refraction-free images with our method.

calibrated with the refraction-free images and finally stereo method is applied. As for the stereo algorithm, OpenCV with NCC based matching cost is applied.

5. EXPERIMENT

5.1. Evaluation using planar object

For the experiment, two light field cameras, Lytro Illum, and water tank of $90 \times 45 \times 45cm$ dimensions are used (Fig. 4). Two cameras are set outside the water tank, and the water tank is filled with clear water. We intentionally slanted the cameras (it looks as if the refractive interface is slanted for the cameras), to make a strong distortion with approximation methods, which is expected to be solved by our technique. We captured calibration board at two distances, such as far and near from the cameras to see the tolerance of proposed algorithm against depth-dependent error. We applied both proposed algorithm as well as approximation-based algorithm [2] to synthesize distortion-free images.

For evaluation, we captured the textured planar board at far, medium and near from the camera. We tested with following four different conditions, such as (a) approximation-based algorithm [2] with far calibration board, (b) approximation-based algorithm [2] with near calibration board, (c) proposed algorithm and (d) proposed algorithm with distortion removal based on [2]. We set number of weighted averaging pixels to 32, and super-sampling ratio to 2. Examples of refraction-free images are shown in Fig. 5. Image synthesis takes 53 milliseconds for our algorithm with Intel Xeon E5640 CPU, which is a realtime process.

After synthesizing refraction-free images using each method, we rectified the images and applied NCC based stereo. Results of disparity maps are shown in Fig. 6. We can observe that the approximation-based algorithms [2] produces moderate results when the target depth is close to the depth of the calibrated tool, however, the results are getting worse, if the target depth is far from the depth of the calibration tool. On the other hand, proposed algorithms produce better results regardless of depth of the target and the cali-

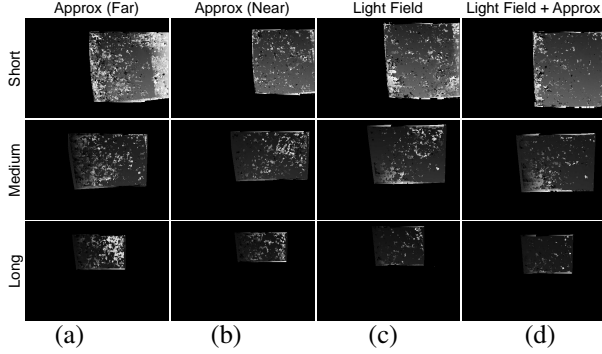


Fig. 6. Results of stereo matching with four methods. (a) and (b): approximation-based algorithm [2]. (c) and (d): proposed algorithm. Noises are decreased in our algorithm.

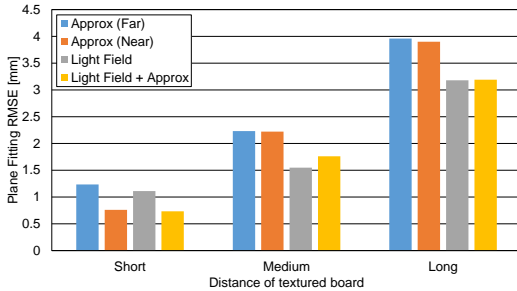


Fig. 7. Results of plane fitting on textured board.

bration board. Fig. 7 shows quantitative evaluation results by plane fitting on reconstructed board after outlier removal, clearly showing that the proposed algorithm outperforms the approximation-based techniques quantitatively.

5.2. Reconstruction of arbitrary shape objects

We tested our method using several objects with complicated texture, such as a crocodile figurine and a ceramic bowl. In this experiment, depth of the calibration board is placed farther than both target objects. Reconstruction results for qualitative evaluation are shown in Fig. 8. We also apply conventional approximation-based algorithm [2] for comparison. We can confirm that the shapes of the approximation-based algorithm is unstable because of the mismatch of the depth between reconstruction and calibration, whereas our technique achieved stable reconstruction for both objects.

6. LIMITATION

In the experiment, we achieved higher accuracy in our algorithm than conventional algorithms. However, in practice, approximation-based algorithm can produce similar/sometimes even better quality than our technique, if refractive interface is precisely orthogonal to the camera axis. We consider this is because our algorithm can produce perfect refraction-free image in theory, however, due to the limitation of the aperture size, image quality can be degraded by the following reason. According to our calculation, possible field-of-view for perfect refraction-free image is 30 degrees, while original field-of-view is about 60 degrees for Lytro Illum. To compensate the problem, we introduce a weighted average of nearby

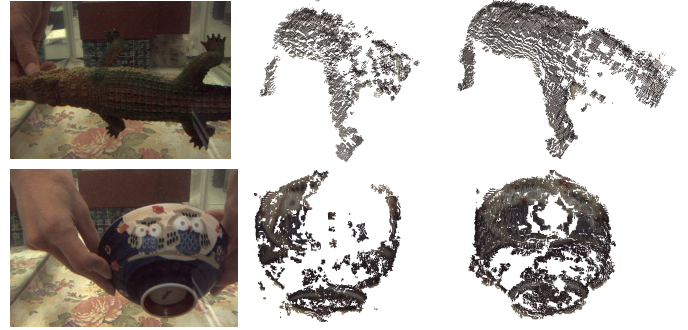


Fig. 8. Qualitative comparison on reconstruction. **Left:** Captured images. **Center:** Results of approximation-based algorithm [2]. **Right:** Results of proposed algorithm.

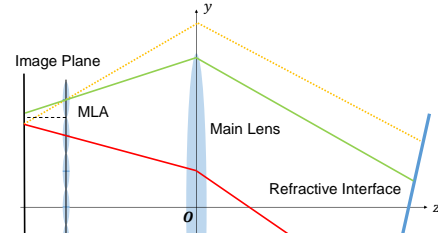


Fig. 9. Illustration of the limitation and compensation by weighted averaging. Since red line ray is observed instead of orange line going outside the aperture, we collect neighbor green line rays to synthesize orange line ray.



Fig. 10. Comparison of synthesized images with different numbers of averaged rays (1, 8, 64, from left to right).

pixels in our method (Fig. 9), which leads a defocus effect producing blur in final image by increasing the number of averaging rays (Fig. 10). Using wider field-of-view for the lens is one promising solution.

7. CONCLUSION

In this paper, we propose an algorithm to synthesize refraction-free image using light field camera. Proposed algorithm enabled geometrically correct image synthesis for any kind of refraction and performed better 3D reconstruction based on stereo than previous approximation-based methods. Moreover, the proposed method is capable of fast-computation, *i.e.*, real-time process with common PC. Although there is a limitation due to the limited size of aperture, our experiments show that our technique is mostly better than previous methods, especially under severe refraction cases. As our future work, we consider underwater single view depth computation is also possible using light field camera, as well as applying the proposed method to active stereo techniques.

8. REFERENCES

- [1] Amit Agrawal, Srikumar Ramalingam, Yuichi Taguchi, and Visesh Chari, “A theory of multi-layer flat refractive geometry,” in *IEEE Conference on Computer Vision and Pattern Recognition*. 2012, IEEE.
- [2] Ricardo Ferreira, João P. Costeira, and João A. Santos, “Stereo reconstruction of a submerged scene,” in *Pattern Recognition and Image Analysis*. 2005, pp. 102–109, Springer.
- [3] Anne Jordt-Sedlazeck and Reinhard Koch, “Refractive structure-from-motion on underwater images,” in *IEEE International Conference on Computer Vision*. 2013, IEEE.
- [4] Ryoichi Kawahara, Shohei Nobuhara, and Takashi Matsuyama, “A pixel-wise varifocal camera model for efficient forward projection and linear extrinsic calibration of underwater cameras with flat housings,” in *IEEE International Conference on Computer Vision Workshops*. 2013, pp. 819–824, IEEE.
- [5] Michael Bleier and Andreas Nüchter, “Low-cost 3d laser scanning in air or water using self-calibrating structured light,” *International Archives of the Photogrammetry, Remote Sensing and Spatial Information Sciences*, pp. 105–112, 2017.
- [6] Hiroshi Kawasaki, Hideaki Nakai, Hirohisa Baba, Ryusuke Sagawa, and Ryo Furukawa, “Calibration technique for underwater active oneshot scanning system with static pattern projector and multiple cameras,” in *IEEE Winter Conference on Applications of Computer Vision*. 2017, IEEE.
- [7] Kazuto Ichimaru, Ryo Furukawa, and Hiroshi Kawasaki, “Multi-scale cnn stereo and pattern removal technique for underwater active stereo system,” in *International Conference on 3D Vision*, 2018.
- [8] Huimin Lu, Yujie Li, Hyungseop Kim, and Seiichi Serikawa, *Underwater Light Field Depth Map Restoration Using Deep Convolutional Neural Fields*, vol. 752, pp. 305–312, Springer, 2018.
- [9] Tingtian Li, Daniel P.K. Lun, Yuk-Hee Chan, and Budianto, “Robust reflection removal based on light field imaging,” *IEEE Transactions on Image Processing*, pp. 1798–1812, 2018.
- [10] Hae-Gon Jeon, Jaeik Park, Gyeongmin Choe, Jinsum Park, Yunsu Bok, Yu-Wing Tai, and In So Kweon, “Accurate depth map estimation from a lenslet light field camera,” in *IEEE Conference on Computer Vision and Pattern Recognition*. 2015, IEEE.
- [11] Yingling Zhang, Peihong Yu, Wei Yang, Yuanxi Ma, and Jingyi Yu, “Ray space features for plenoptic structure-from-motion,” in *IEEE International Conference on Computer Vision*. 2017, IEEE.
- [12] Kiriakos N. Kutulakos and Eron Steger, “A theory of refractive and specular 3d shape by light-path triangulation,” *International Journal of Computer Vision*, vol. 76, pp. 13–29, 2008.
- [13] Gordon Wetzstein, David Roodnick, Wolfgang Heidrich, and Ramesh Raskar, “Refractive shape from light field distortion,” in *IEEE International Conference on Computer Vision*. 2011, IEEE.
- [14] Katherine A. Skinner and Matthew Johnson-Roberson, “Towards real-time underwater 3d reconstruction with plenoptic cameras,” in *IEEE International Conference on Intelligent Robots and Systems*. 2016, IEEE.